A MODEL FOR THE OPERATION ANALYSIS OF HIGH SPEED UNIVERSAL MOTORS WITH TRIAC REGULATED MAINS VOLTAGE SUPPLY

Antonino Di Gerlando, Roberto Perini

Dipartimento di Elettrotecnica, Politecnico di Milano - Italy
antonino.digerlando@polimi.it; roberto.perini@polimi.it

Abstract

The universal motor, used in low cost, large scale household appliances, is analysed, developing its transient model, which takes into account saturation effects: it allows to analyse the performances and waveforms at the load side (torque, speed) and at the terminals (voltage, current). The TRIAC regulation of the feeding mains voltage is considered, evaluating the distortion effects in different operating conditions.

1.- INTRODUCTION

The commutator universal motor (UM), whose main features are well known, is still largely used in several small rating home and commercial appliances, for its appreciated features of low cost and simple regulation possibilities, that make this machine again a competitive component, compared with other motors and drives.

Nevertheless, the increasing competition of alternative solutions leads to better the knowledge of this series field excited motor, in order to attain design and construction improvements [11-14] and to allow a more accurate energy and waveform performance estimation, both as regards load side behaviour and mains interface.

In fact, even if the operation principle of the UM has been known for a long time, its model refinement is still in progress, using FEM and/or circuit approaches [1-10], mainly with the aim to deepen the various and complicated phenomena occurring during operation.

In the present paper, the analysis (of general value, based on a circuit approach) will be applied to high speed UMs used in vacuum cleaners, with maximum speeds up to and above forty thousands r.p.m..

These motors are frequently equipped with a simple, low cost, speed regulator, consisting of a TRIAC, operating a reduction of the mains voltage r.m.s. value.

After the motor model description, limited to the global operation and disregarding the commutation phenomena, the TRIAC regulation will be considered, in order to analyse performances and waveforms in different operating conditions, also estimating the line current distortion, comparing it with the imposed Standard limits.

2.- MOTOR MAIN PARAMETERS AND MODEL

Core geometry and data of the considered motor, commercially available, are shown in fig.1 and Table I.

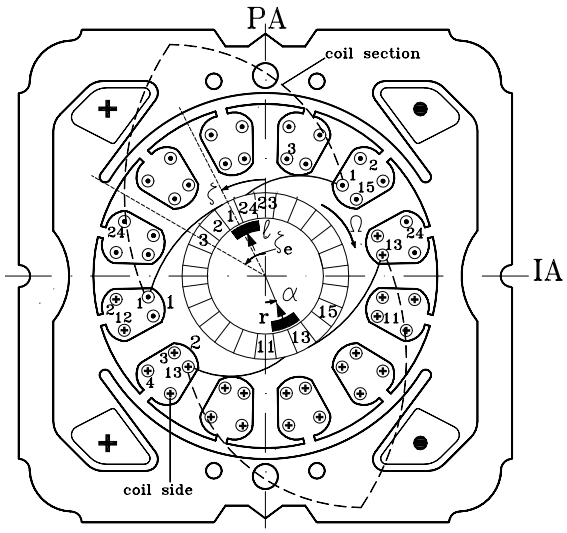

Fig.1 – Structure of the analysed universal motor.

Table I – Main quantities of the analysed universal motor

V_n [V]; I_n [A]; $P_{in\ n}$ [kW]	220;5.8; 1.25
f_n [Hz]; N_n [r.p.m.]	50; 32,000
poles p; N° of commutator segments k	2; 24
N° of slots c; coil sides/(layer-slot): u; rotor winding parallel paths: a = p	12; 2; 2
rotor turns N°: N_a; wire ∅ [mm]	360; 0.40
field turns N° per pole: N_f; wire ∅ [mm]	130; 0.63
pitch shortening ε; brush shifting α	30°; 22.5°
Brush sizes: b · w · h [mm]	6.3·10.95·37
brush – segments contact ratio β	1.96
rotor diameter [mm]	38.25
air gap δ; axial length; lam.width [mm]	1.47; 32; 0.5

Called $m_f = N_f \cdot i_m$ the field magnetizing m.m.f., it can be shown that, due to the series connected armature reaction, the total m.m.f. $m_p(\zeta)$ acting under the pole, in the generic angular position ζ of fig.1, equals:

$$m_p(\zeta) = m_f \cdot (1 + \sigma \cdot (\zeta - \alpha)),\ \sigma = (N_a/N_f)/(2\cdot\pi). \quad (1)$$

(1) leads to evaluate the pole flux φ_m (by magnetic circuit solution or via FEM analysis) for various values of the magnetizing line current i_m: the result is shown in fig.2, together with the unsaturated curve $\varphi_{mo} = \Lambda_o \cdot m_f$.

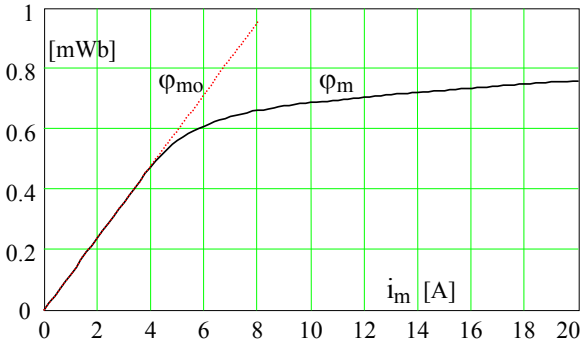

Fig.2 – Magnetization characteristic of the motor of Table I.

Evaluating the armature flux linkage and applying the Faraday's law allows to obtain the total rotor e.m.f., as measured at the brushes (e_{at}, e_{as} are the transformer and speed e.m.f. respectively):

$$e_a = e_{at} + e_{as} = N_a \cdot C_{at}(\varepsilon,\alpha) \cdot d\varphi_m/dt + N_a \cdot C_{as}(\varepsilon,\alpha)\, \varphi_m \cdot \Omega \quad (2)$$

where C_{at} and C_{as} are linkage coefficients (for the motor of Table 1, it follows: $C_{at} = -0.059$; $C_{as} = 0.31$). By defining

$$\Lambda_a = \varphi_m / m_f \quad (3)$$

$$\Lambda_d = d\varphi_m / dm_f \quad (4)$$

apparent and differential permeances (fig.3), (2) becomes:

$$e_a = e_{at} + e_{as} = L_{da}(i_m) \cdot di_m/dt + M(i_m) \cdot i_m \cdot \Omega \quad (5)$$

where $L_{da}(i_m) = N_a \cdot N_f \cdot C_{at} \cdot \Lambda_d(i_m)$ (6)

and $M(i_m) = N_a \cdot N_f \cdot C_{as} \cdot \Lambda_a(i_m)$. (7)

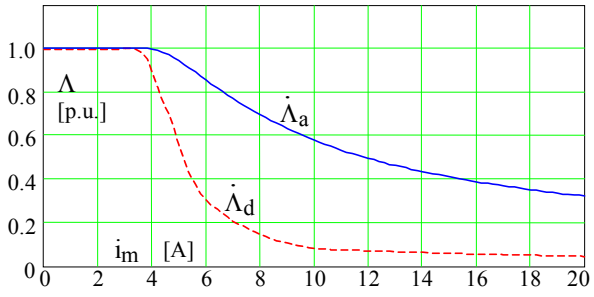

Fig.3 – Apparent and differential permeance, in p.u., referred to the unsaturated permeance Λ_o ($\Lambda_o = 0.92$ μH).

As regards the e.m.f. induced by the pole flux φ_m in the two field coils, we can write:

$$e_f = 2 \cdot N_f \cdot d\varphi_m/dt = L_{df}(i_m) \cdot di_m/dt \quad , \quad (8)$$

with $L_{df}(i_m) = 2 \cdot N_f^2 \cdot \Lambda_d(i_m)$. (9)

Besides the e.m.f.s induced by the pole flux φ_m, the motor model must include the leakage inductive voltage drops (due to $L_{\ell f}$, $L_{\ell a}$: leakage field and armature inductances) and the resistive voltage drops (across the field and armature resistances R_f and R_a and due to the brushes, v_b).

Moreover, the core losses should be considered:

- the stator core losses depend only on the feeding frequency, while the rotor core losses depend also on the internal frequency, proportional to the speed Ω;
- the core loss dependence on the local peak flux densities squared can be expressed in terms of pole flux squared: thus, the core losses can be considered non linearly dependent on the peak magnetizing line current $I_{m.peak}$.

A possible core loss model could be a conductance G_c, derived at the input terminals: $G_c = G_c(\Omega, I_{m.peak})$.

Therefore, the detailed equivalent circuit of the motor is represented in fig.4: as shown, the feeding voltage v equals the sum of the field and armature voltages, v_f and v_a.

The circuit of fig. 4 has a general validity, and it can be used for the performance analysis of any UM.

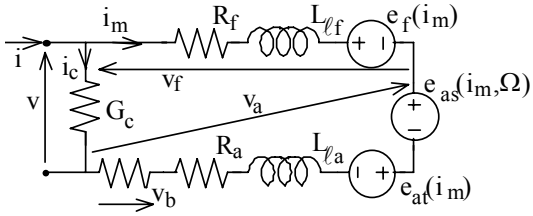

Fig.4 – Detailed equivalent circuit of the universal motor.

In our case, being mainly interested in evaluating the line current waveform and distortion in different conditions, the core losses current component can be considered negligible: thus, by some manipulations and parameter aggregations, the global circuit of fig.5 can be used, where:

$$R = R_f + R_a + R_b \quad , \quad (10)$$

$$L(i_m) = L_{df}(i_m) + L_{da}(i_m) + L_{\ell f} + L_{\ell a} \quad . \quad (11)$$

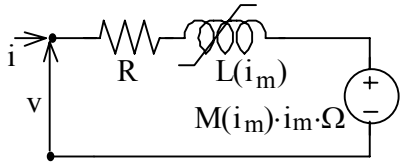

Fig.5 – Simplified equivalent circuit of the universal motor.

Besides the circuit quantities, the electromagnetic torque expression $T_e(i_m)$ must be considered, given by:

$$T_e(i_m) = M(i_m) \cdot i_m^2 \quad . \quad (12)$$

The electromagnetic torque characteristic, shown in fig.6, initially parabolic, has the typical saturated shape.

In our case, the load at the motor shaft is given by the vacuum cleaner fan, whose air flow is effectively exploited also for the motor cooling; the load equation is given by:

$$T_\ell(\Omega) = T_o + k_T \cdot \Omega^2 \quad . \qquad (13)$$

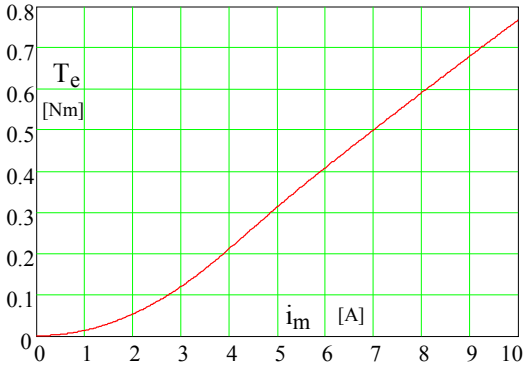

Fig.6 – Electromagnetic torque, as a function of the current.

2.- WAVEFORMS ANALYSIS

Considering the electrical and mechanical differential equations, the time domain analysis can be performed; in particular, it is worth to study the steady-state behaviour, both as regards the mechanical and electrical waveforms, and concerning some energetic performances.

In case of direct sinusoidal voltage feeding (with V_{line} = 220 V_{rms}, 50 Hz, or with TRIAC regulation with a zero firing delay control), the steady state simulation results give the waveforms shown in fig.7.

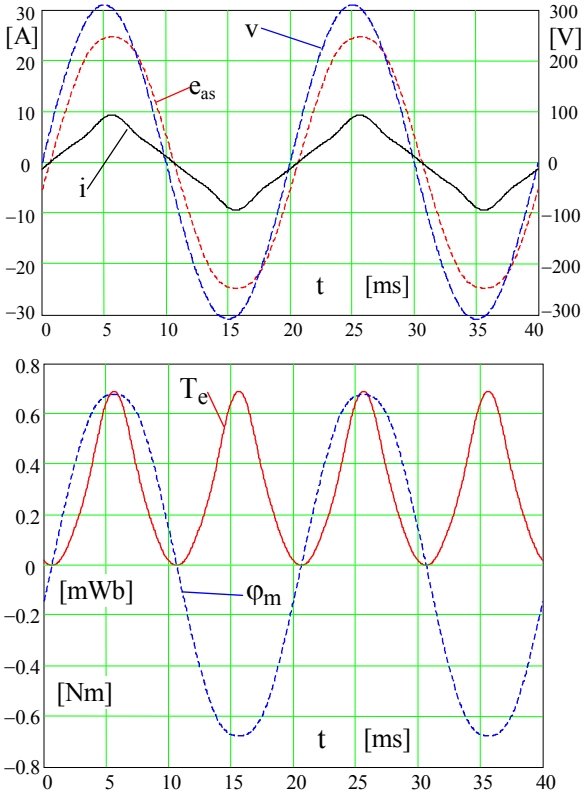

Fig.7 – Waveforms at steady state operation with sinusoidal voltage feeding: V = 220 V_{rms}, 50 Hz:
above: line voltage v and current i, speed e.m.f. e_{as};
below: pole flux φ_m, electromagnetic torque T_e.

Now consider a TRIAC phase control: for example the waveforms of fig.8 refer to a steady-state operation with a firing delay of 110° (with the previous mains conditions).

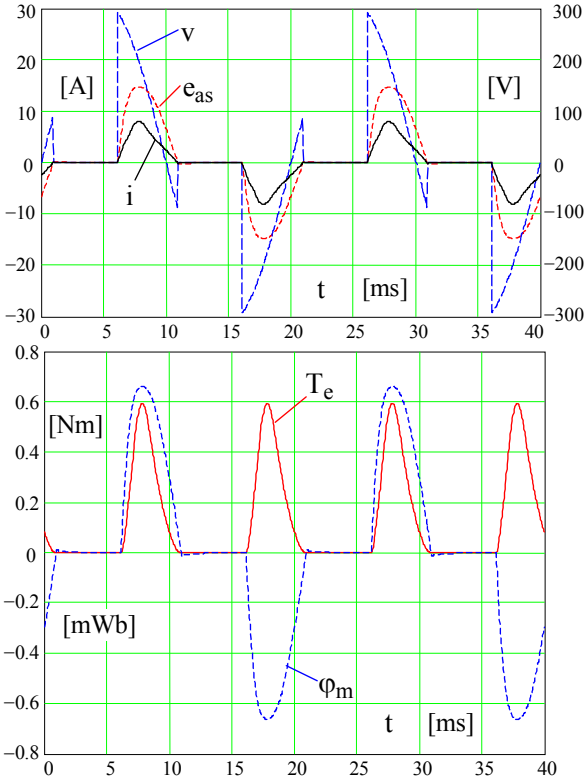

Fig.8 – Waveforms at steady state operation with mains feeding and phase control (110°): V = 220 V_{rms}, 50 Hz:
above: line voltage v and current i, speed e.m.f. e_{as};
below: pole flux φ_m, electromagnetic torque T_e.

The following remarks can be applied:

- with sinusoidal voltage feeding, the line current appears distorted, because of saturation, while both the pole flux φ_m and the speed e.m.f. e_{as} remain roughly sinusoidal; the electromagnetic torque has the typical double frequency shape, with average value $T_{e.ave}$ = 0.30 Nm; the average speed equals N_{ave} = 31,300 r.p.m.;
- with mains voltage feeding, reduced by a TRIAC phase control equal to 110°, all the electrical quantities are significantly distorted: in particular, the current consists of two alternated pulses with large zero current intervals; the speed e.m.f. and pole flux are not sinusoidal any more: as known, the desired effect of the phase control is to reduce the average torque (here $T_{e.ave}$ = 0.13 Nm) and, consequently, the average speed (equal to 19,100 r.p.m.).

As already discussed about the waveforms of fig.7, even in case of sinusoidal voltage feeding, the input current is distorted, due to the significant core saturation.

Fig.9 shows the corresponding histogram of the rms values of the odd harmonic currents; the limits imposed by

the Standards [15] for the odd harmonics are also reported, with reference to a Class A device with input current less than 16 A_{rms}: the distortion is due to the low order harmonics (mainly up to the ninth order, particularly the third); in spite of a significant THD value (14.3%), the limits are largely observed.

Fig.10 shows a similar histogram for mains feeding via TRIAC, with a phase control of 110°, already considered in the waveforms of fig.8: here, the THD is very high (71.0%), but the Standard limits are again respected; also in this case, the most significant harmonics appear to be the low order ones, up to the ninth one.

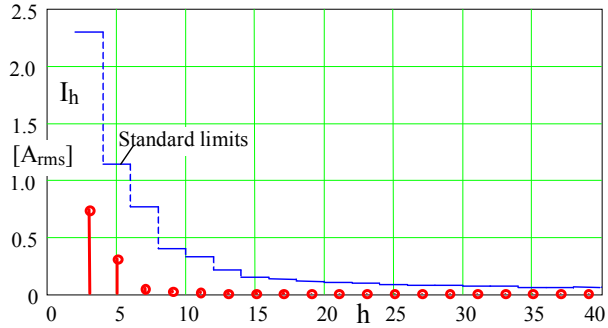

Fig.9 – Rms harmonic currents absorbed by the motor of Table I, for sinusoidal feeding in rated conditions (bars); Standard limits for the input current harmonics [15] (stepped curve).

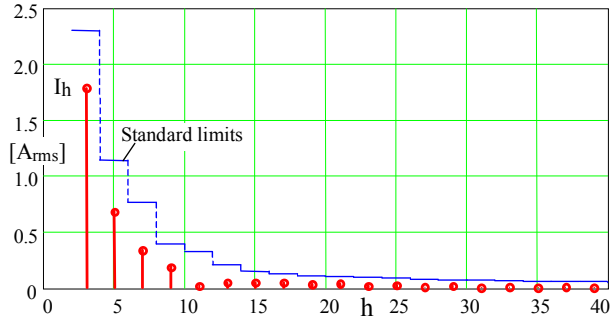

Fig.10 – Rms harmonic currents absorbed by the motor of Table I: mains feeding via TRIAC; phase control = 110° (bars); input current harmonics Standard limits [15] (stepped curve).

3.- PERFORMANCE EVALUATIONS

In the following diagrams, obtained by the steady-state solution of the model differential equations, the useful regulation range of the TRIAC phase control θ_{pc} will be examined (0-150°), considering the most important aspects of interaction with the mains and the main motor performance quantities.

Fig.11 shows the curves of the rms value of the fundamental and of the odd harmonic currents, together with the curve of the total rms input current, as a function of the phase control angle θ_{pc}; the corresponding Standard limits $I_{h\ell}$ for the harmonic currents [15] are also evidenced; the following remarks can be made:

– with no phase control (corresponding to direct mains feeding), the harmonic distortion is low, but not zero, because of the distorting effect due to saturation (particularly as regards the third harmonic component);
– with low phase control angles, the fundamental current and the harmonic components remain roughly stationary, at first because the phase control does not operate under the natural motor phase displacement, and because of the weak effects of small θ_{pc} values;
– the harmonic currents, especially the third order one, become important above 40°, reaching the maximum absolute values for control angles around 80°-90°;
– the maximum values of the harmonic currents remain under the corresponding Standard limits $I_{h\ell}$, even if the distortion margins are quite small, especially as regards the third harmonic component;
– the reduction of the total rms current I_{tot} as a function of θ_{pc} is similar to the behaviour of the fundamental component I_1, showing higher values, caused by the important rms value of the current harmonic residual.

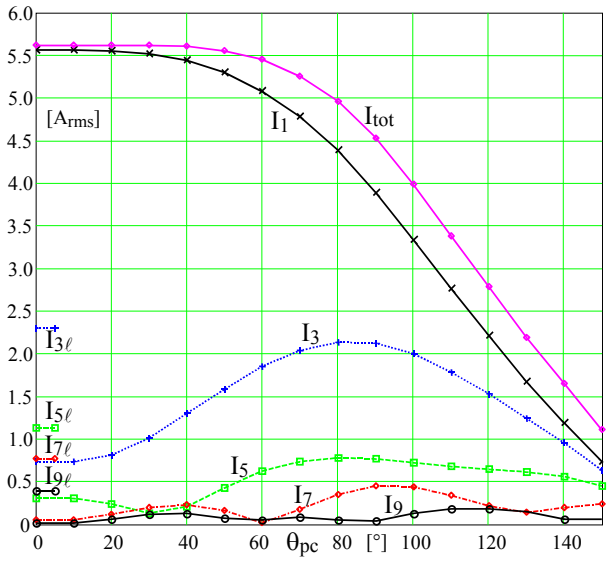

Fig.11 - Curves of the rms value of the fundamental and of the odd harmonic currents, together with the curve of the total rms input current, as a function of the phase control angle θ_{pc}; the corresponding Standard limits $I_{h\ell}$ for the harmonic currents [15] are also evidenced.

Fig.12 shows the variation of the average value of the electromagnetic torque T_e and of the motor speed N, as a function of the phase control angle θ_{pc}: both T_e and N are expressed in p.u., referred to the corresponding values with direct mains feeding, θ_{pc} = 0 ($T_{e\text{-}ref}$ = 300 mNm; N_{ref} = 31300 rpm); one can observe that:

– the torque and speed regulation is a non-linear function

of the phase control angle θ_{pc};

– the speed decrease with the phase control increase is slower than the torque reduction;
– the initial regulation range is weakly effective in lowering the speed: for example, a phase control of 70° reduces the motor speed of 10% only;
– the speed is halved with a phase control of roughly 125°: for it, the torque is about 25% of the rated one.

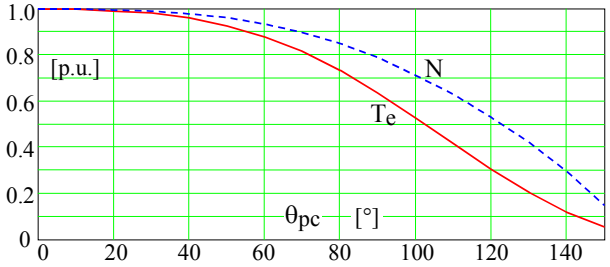

Fig.12- Average electromagnetic torque T_e and speed N as a function of the phase control angle θ_{pc} (T_e and N in p.u., referred to the values with sinusoidal feeding operation (corresponding to θ_{pc}= 0): $T_{e\text{-}ref}$ = 300 mNm; N_{ref} = 31,300 rpm).

As already observed, the increase of the phase control angle causes an important increase of the current distortion: apart from the harmonic pollution limits, the increasing weight of the current harmonics produces higher electrical losses, compared with those corresponding to operation with sinusoidal current.

Fig.13 shows the ratio among the total Joule winding electrical losses $P_{\ell e}$, including the harmonic losses, and the Joule winding electrical losses $P_{\ell e1}$, due to the fundamental component only, being the control angle θ_{pc} the same: this loss ratio increases very much above θ_{pc} = 70°, when the speed regulation becomes important.

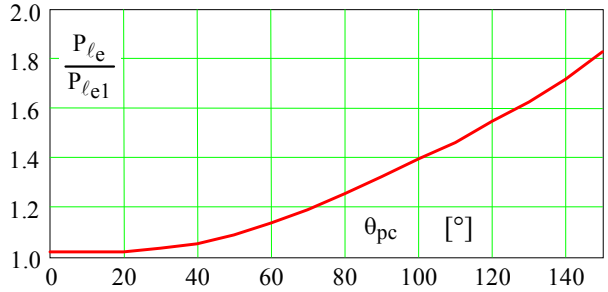

Fig.13 – Ratio among total Joule electrical losses and fundamental component losses (phase control angle being the same)

On the other hand, the electrical loss ratio $P_{\ell e}/P_{\ell e1}$ is not completely representative of the energetic behaviour of the TRIAC fed motor: in fact, the losses must be compared with the actual output power, in order to appreciate the consequences in terms of efficiency reduction. To this aim, fig.14 shows the curves of the ideal output power (core and mechanical losses not included) and of the Joule winding electrical losses (considering or not the harmonic effects), as a function of the control angle; one can observe that:

– after a first range of practical constancy, the output power decreases, showing the maximum falling rate in the phase control range 70°-120°;
– the total electrical losses $P_{\ell e}$ diminishes too, as like as the electrical losses due to the fundamental component $P_{\ell e1}$, as the phase control increases;
– thus, even if the ratio $P_{\ell e}/P_{\ell e1}$ increases, the extra energy consumption caused by the harmonic content tends to become negligible.

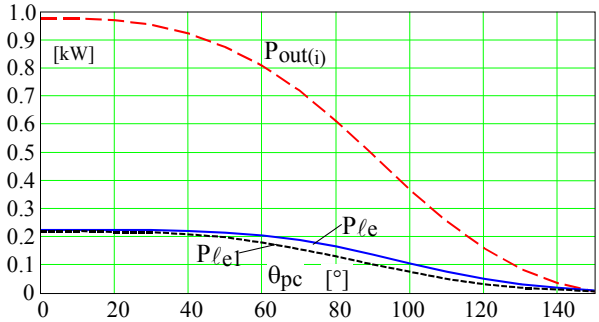

Fig.14 – Curves of the ideal output power $P_{out}(i)$ (core and mechanical losses non included) and of the total $P_{\ell e}$ and fundamental $P_{\ell e1}$ Joule winding electrical losses, as a function of the control angle θ_{pc}.

Another important operating quantity, that qualifies the behaviour of the TRIAC-motor system towards the mains, is the power factor PF; fig.15 shows the dependence of the PF on the phase control, together with the trend of the two factors forming the PF, that is the displacement factor DF and the distortion factor ν.

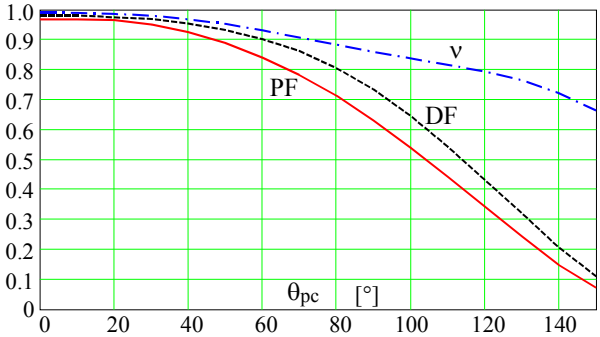

Fig.15 – Dependence of the power factor PF on the control angle θ_{pc}; curves of the displacement factor DF and of the distortion factor $\nu = I_1/I_{tot}$; as known, PF = DF·ν.

The following remarks can be made:

– in case of zero or low phase control, the natural PF of the UM is good, well above 0.9;
– when increasing the phase control, PF decreases importantly, with a dramatic fall above θ_{pc} = 80°;
– the cause of the great PF reduction is only partially

linked to the decrease of the distortion factor ν;

– the main reason of the PF worsening is the great reduction of the displacement factor, caused by the increase of the phase angle among the waveforms of the fundamental of current and of the line voltage.

On the other hand, as already observed as regards the electrical losses, also the energetic quantities included in the PF reduce their actual values when increasing the phase angle control, thus partially mitigating the impact of the PF lowering.

In fact, coming back to the curve of the total line current I_{tot} of fig.11, one can conclude that the apparent power absorbed for a phase control angle equal to $\theta_{pc} = 150°$ is roughly 20% of that absorbed with no phase control. Even if this amount cannot be considered negligible, its real relevance in term of effective degradation of energetic behaviour is reduced; moreover, the importance of this low PF condition must be considered also in term of time duration of performances at low speed, compared with the duration of the high speed operation.

4.- CONCLUSIONS

In the paper, a transient model of the universal motor has been developed, taking into account the constructional quantities of the machine, known from the design stage, and the effect of the saturation phenomena on the equivalent circuit parameters.

This model has been completed with the model of the load that, in the considered case, consists of the fan of a vacuum cleaner, operating also as a cooling system.

The operation with direct sinusoidal mains feeding has been analysed, together with that of the machine fed via a simple TRIAC static converter.

Some operating conditions have been considered, examining the electrical and mechanical waveforms, under TRIAC feeding regulation: the current distortion has been evaluated, comparing the harmonic spectrum with the Standard limits, as a function of the phase control.

Finally, the trend of the output power and of the electrical losses has been analysed, together with the values of the power factor.

Preliminary experimental tests have shown a good agreement with the simulation results: a more complete theoretical and numerical analysis, together with a systematic series of tests, will be the subject of further research activities.

ACKNOWLEDGEMENT

This work has been supported by the Italian National Ministry of Education, University and Research (MIUR), Grant Cofin 2001, Title: “Improvement of the energy efficiency of electrical motors and drives for industrial and civil applications”.

REFERENCES

[1] Matsuda T. et al.: *Method for analysing the commutation in small universal motors*, IEE Proc. on Electrical Power Applications Vol. 142, n° 2 March 1995.

[2] Fujii T, Hazanawa T.: *Commutation of universal motors*, IEEE IAS Annual Meeting 1989, Conf. Record vol. 1.

[3] Fujii T.: *Study of universal motors with lag angle brushes*, IEEE Trans. on P.A.S., Vol. PAS-101, n° 6 June 1982.

[4] Wang Ren H., Walter R.: *Computer aided simulation of performances and brush commutation for universal motors with two coils per armature slot*, Intern. Conference on Electric Machines and Drives IEMD '99 pg. 559-561.

[5] Ebben R., Brauer J., Cendes Z., Demerdash N.: *Prediction of performance characteristics of a universal motor using parametric Finite Element Analysis*, Intern. Conference on Electric Machines and Drives IEMD '99 pg. 192-194.

[6] Ping Zhou, Brauer J., Stanton S., Cendes Z.: *Dynamic modelling of universal motors*, International Conference on Electric Machines and Drives IEMD '99 pg. 419-421.

[7] Bradley K. J., Ismail W. M. H.: *The performance analysis of the single-phase, a.c. commutator motor*, The 5th International IEE Conference on Electrical Machines and Drives, Session 5B, paper 3, London 1991.

[8] McDermott T., Zhou P., Gilmore J., Cendes Z.: *Electromechanical system simulation with models generated from FE solutions*, IEEE Trans. on Mag.,v.33, N2, March 1997.

[9] Wang, R.H.; Walter, R.T., *Modeling of universal motor performance and brush commutation using finite element computed inductance and resistance matrices*, IEEE Trans. on Energy Conversion, Vol.15 Issue: 3 , Sept. 2000.

[10] Costa, M.C.; Nabeta, S.I.; Cardoso, J.R.: *Modified nodal analysis applied to electric circuits coupled with FEM in the simulation of a universal motor* , IEEE Trans on Mag Vol. 36 Issue: 4 Part: 1 , July 2000

[11] Jack, A.; Mecrow, B.; Dickinson, P.; Jansson, P.; Hultman, L.: *Design and testing of a UM using a soft magnetic composite stator*, IEEE IAS Conf. 2000, vol.1

[12] Bencdicic, B.; Kmecl, T.; Papa, G.; Korousic-Seljak, B.: *Evolutionary optimization of a UM*, IECON '01: 27th Industrial Electronics Soc. IEEE Annual Conf., Vol.1, 2001

[13] Korousic-Seljak, B.; Papa, G.; Benedicic, B.; Kmecl, T.: *Improving the technical quality of a UM using an evolutionary approach* **,** Proc 27th Euromicro Conf., 2001.

[14] Cros, J.; Viarouge, P.; Chalifour, Y.; Figueroa, J.: *A new structure of UM using soft magnetic composites*, 36th IAS Annual Meeting Conf. Record, vol.1, 2001.

[15] IEC 1000-3-2 EMC: Part 3, Section 2: *Limits for current emission (equipment input current <16 A per phase),* 1995; consolidated Edition 1998.